PAPER

Check for updates

A tunable phosphorescence supramolecular switch by an anthracene photoreaction in aqueous solution†‡

Ting Su, Yao-Hua Liu, Yong Chen and Yu Liu ⓘD *

Purely organic room-temperature phosphorescence (RTP) has attracted tremendous attention, but is rarely reported to possess stimulus responsiveness. Herein, we report a supramolecular RTP switch based on a dicationic guest molecule (**BPA**) and cucurbituril. **BPA** possesses a photosensitive 9,10-diphenylanthracene core and terminal 4-(4-bromophenyl)pyridium, which can form 1:4 supramolecular assembly with cucurbit[7]uril (**CB[7]**) and an *n*:*n* linear supramolecular polymer with cucurbit[8]uril (**CB[8]**). The assemblies can exhibit tunable fluorescence emission after undergoing a photoreaction of the anthracene unit in **BPA**. It is interesting that **CB[8]** can bind two bromophenylpyridinium units to form a green phosphorescent switch. Notably, the RTP of the assemblies can be reversibly switched on/off by UV irradiation or heating through a tunable Förster resonance energy transfer from 4-(4-bromophenyl)pyridium to anthracene. Moreover, the addition of cucurbituril can significantly accelerate the photoreaction rate of anthracene and enable the assembly to respond quickly to UV irradiation, which expands the application potential of this strategy in stimulus responsive RTP materials.

Introduction

In recent years, purely organic room-temperature phosphorescence (RTP) has gained increasing research interest because of its inherent advantages including a triplet state, longer lifetime and larger Stokes shift.[1–4] Therefore, RTP materials have been widely explored for potential applications in light-emitting devices,[5–7] biological imaging,[8–12] information encryption,[13–16] chemical sensing,[17–21] *etc.* However, purely organic molecules also have some disadvantages, such as low efficiency intersystem crossing (ISC), weak spin–orbit coupling, easy non-radiative transition, and collision quenching by oxygen or impurities, leading to hardly effective phosphorescence emission at room temperature.[22–25] In order to solve the above problems, many strategies to achieve RTP have been proposed, including the introduction of heavy atoms,[26,27] crystalline packing,[28–30] polymerization modification,[31–33] embedding into a matrix,[34–38] molecular aggregation[39,40] and so on.

Among them, a supramolecular method based on macrocyclic compounds has recently attracted great attention in the construction of RTP systems,[41–44] because macrocyclic compounds with hydrophobic cavities can specifically bind guest molecules and induce their RTP effect by virtue of a variety of noncovalent interactions, including hydrophobic effect, electrostatic interactions, hydrogen bonding, and van der Waals interactions.[45–47] The combination of macrocyclic hosts and modified guests can bring the following benefits to purely organic RTP: (1) the rigid environment of macrocyclic compounds can tightly bind the guest, limit its molecular vibration, and reduce the nonradiative transition of the triplet state;[48,49] (2) the hydrophobic cavity can protect the wrapped phosphor from the quenching effect of the external oxygen, water and other impurities.[50,51] Based on the above advantages, many efforts have contributed to the application of supramolecular macrocycles in purely organic RTP systems.[52–54] Tian and co-workers reported an approach to achieve amorphous purely organic RTP small molecules by modifying different phosphors onto β-cyclodextrin, which could suppress the non-radiative relaxation *via* intermolecular hydrogen bonding.[41] Recently, we reported that by modifying bromophenylpyridinium on hyaluronic acid and co-assembling with cucurbit[8]uril (**CB[8]**), a type of macrocycle formed by the polymerization of glycoluril and formaldehyde,[55,56] the resultant supramolecular assembly exhibited good RTP behavior in aqueous solution, which was successfully applied to mitochondrial-targeted imaging of cancer cells.[57] Ma *et al.* constructed a water-soluble tunable RTP system excited by visible light *via* 2:2 supramolecular assembly of triazine/bromophenylpyridinium with **CB[8]** in aqueous solution.[58] These outstanding studies inspire the application

*College of Chemistry, State Key Laboratory of Elemento-Organic Chemistry,
Nankai University, Tianjin 300071, P. R. China. E-mail: yuliu@nankai.edu.cn*

† Dedicated to Professor Daoben Zhu on the occasion of his 80th birthday.
‡ Electronic supplementary information (ESI) available: Experimental procedures, methods for synthesis, relevant characterization details, and supporting photographs. See DOI: 10.1039/d1tc04100b
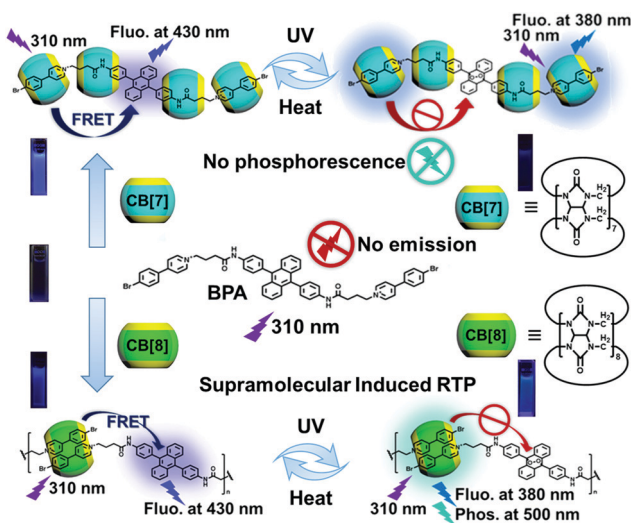
Scheme 1 Illustration diagram of purely organic RTP activated by a photoreaction.

and development of supramolecular macrocyclic compounds in the construction of purely organic RTP systems. However, there are few reports on purely organic RTP molecular switches with stimulus responsiveness.[59–61] Ma and Ding *et al.* realized photo-controllable purely organic RTP based on the photochromic polymer by synthesizing two polymers containing hexaaryl-diimidazole and using their reversible homolysis to form triphenylimidazole radicals under UV irradiation.[62]

Herein, we wish to report a photoreaction-driven RTP supramolecular switch based on cucurbituril and a dicationic guest molecule possessing a photosensitive 9,10-diphenylanthracene core and terminal 4-(4-bromophenyl)pyridium (**BPA,** Scheme 1). Interestingly, this 9,10-diphenylanthracene derivative **BPA** can form not only 1:4 supramolecular assembly with cucurbit[7]uril (**CB[7]**) but also 1:1 supramolecular linear assembly with **CB[8]**, where 4-(4-bromophenyl)pyridium moieties are encapsulated by a **CB[8]** cavity in a head-to-tail manner to form biaxial pseudorotaxane. However, 9,10-diphenylanthracene can directly absorb energy from the first excited singlet state of 4-(4-bromophenyl)pyridium by the mechanism of Förster resonance energy transfer (FRET) and block the ISC process, leading to the inhibition of the production of RTP.[63,64] In response to UV irradiation, **BPA** can promote the production of singlet oxygen and combine with it to form endoperoxides (**BPA_{EPO}**). This combination can be broken reversibly after being heated, so that the molecule can return to its initial reduced state. After the conjugated structure of 9,10-diphenylanthracene is destroyed by a photoreaction, the fluorescence and green phosphorescence of the 4-(4-bromophenyl)pyridium group appear. These results are attributed to the strong supramolecular interaction between **CB[8]** and **BPA**, which promotes the ISC pathway, limits molecular motion to suppress the nonradiative transition, and reduces the collision of phosphorescent triplets with triplet oxygen and other impurities. Significantly, the addition of supramolecular macrocycles can accelerate the photoreaction process and shorten the time for guest molecules to combine with singlet oxygen in aqueous solution to

form endoperoxides. Such acceleration behavior is helpful to realize the sensitive response to UV irradiation in practical applications and provides a more reliable application prospect for this strategy.

Results and discussion

Synthetic routes of the guest molecules, *i.e.* a phosphor group 4-(4-bromophenyl)pyridium modified 9,10-diphenylanthracene derivative and its photoreaction product endoperoxide, are summarized in Scheme S1 (ESI‡). The dicationic guest molecule **BPA** was obtained in a total yield of >52% after the salinization between the 9,10-diphenylanthracene derivative **2** and 4-(4-bromophenyl)pyridium and characterized by NMR and mass spectra (Fig. S1–S6, ESI†). According to previous reports, cucurbituril can be used to bind the phosphorescent group 4-(4-bromophenyl)pyridium containing positive charges, enhance its solid phosphorescence intensity and induce visible solution phosphorescence.[57,65] In order to explore the influence of the host–guest interaction on the optical properties of **BPA**, we select two cucurbituril macrocycles **CB[7]** and **CB[8]** for subsequent experiments. Job's plot measured by UV-vis absorption and fluorescence emission demonstrates that the stoichiometric ratios of **BPA** : **CB[7]** and **BPA** : **CB[8]** are 1 : 4 and 1 : 1, respectively (Fig. S13, ESI‡). The two-step binding constants of **BPA** with **CB[7]** measured by UV-vis absorption titration are $K_{a1} = 1.53 \times 10^6$ M^{-1} and $K_{a2} = 5.69 \times 10^5$ M^{-1}, and the one-step binding constant of **BPA** with **CB[8]** is $K_a = 9.39 \times 10^6$ M^{-1} (Fig. S14, ESI‡). Moreover, ^{1}H NMR experiments were carried out to further investigate the host–guest binding mode between **BPA** and **CB[7]**/**CB[8]** (Fig. S15, ESI‡). As shown in Fig. S16 (ESI‡), the addition of **CB[7]** can passivate and weaken the H_d, H_e, H_f and H_g signals of 4-(4-bromophenyl)pyridinium and create new peaks in a higher field, indicating that the bromophenylpyridinium moieties of **BPA** are incorporated into the cavity of **CB[7]**. With the addition of >1 equivalent **CB[7]**, the hydrogen peak assigned to H_a and H_c protons shifted to a lower field, indicating that the alkyl chain of **BPA** is also partly included in the **CB[7]** cavity. In the case of **CB[8]**/**BPA** assembly (Fig. S17, ESI‡), significant ^{1}H NMR signal passivation of **BPA** protons is observed, whose degree gradually deepens with an increase of the **CB[8]** concentration. Meanwhile, when fixing the host–guest ratio at 1 : 1 and reducing the total concentration (Fig. S18, ESI‡), the changes in the peak shape and position are observed, indicating that supramolecular polymers may be formed. In the 2D ROESY (rotating-frame Overhauser effect spectroscopy) spectrum of **BPA** in the presence of 1 equiv. of **CB[8]** (Fig. S19, ESI‡), a strong ROE cross-peak between H_e and H_f is observed. According to our previous studies on bromophenylpyridinium derivatives, it is speculated that the two bromophenylpyridinium parts may be wrapped into the cavity of **CB[8]** in a head to tail orientation.[66] In the 2D DOSY spectra (Fig. S20, ESI‡), the self-diffusion coefficient of **BPA** decreases from 1.255×10^{-10} to 7.896×10^{-11} m^2 s^{-1} after adding **CB[8]**, indicating the formation of a large assembly. In addition, we synthesize a model molecule **BPB** (Scheme S2 and

2624 | *J. Mater. Chem. C*, 2022, **10**, 2623–2630

This journal is © The Royal Society of Chemistry 2022

Fig. S10–12, ESI‡) to simulate the interaction between the two arms of **BPA** and cucurbituril. Job's plot of the **CB[7]/BPB** system measured by the UV-vis absorption method confirms the optimal binding ratio of **CB[7]** to **BPB** as 2:1, and the two-step binding constants are $K_1 = 6.93 \times 10^6$ M^{-1} and $K_2 = 3.70 \times 10^6$ M^{-1}, respectively (Fig. S21, ESI‡), which are in the same order of magnitude as the interaction between **BPA** and **CB[7]**. By comparing the ^{1}H NMR spectra of **BPB** and its host–guest complex (Fig. S22, ESI‡), it is found that the hydrogen peak of the bromophenylpyridinium moiety is seriously passivated, and a new set of peaks appear at a higher field with the addition of **CB[7]**. This phenomenon confirms the existence of the host–guest interaction in a slow exchange manner. With the addition of a gradient concentration of **CB[7]** (Fig. S23, ESI‡), the peak of **BPB** decreases gradually, and a new peak at a higher field is observed. When 2 equivalents of **CB[7]** are added, the original peak disappears completely, indicating that the binding ratio of **BPB** to **CB[7]** is 1:2. Moreover, the MALDI-TOF mass spectrum also shows the peak assigned to the 1:2 inclusion complex between **BPB** and **CB[7]** at m/z = 2722.764 (Fig. S24, ESI‡). The addition of **CB[8]** can also make the peak of the aromatic hydrogen of **BPB** shift to a higher field (Fig. S25, ESI‡). Then, the morphology of the assembly is characterized using a scanning electron microscope (SEM, Fig. S26, ESI‡), where **BPA** forms a folded film structure on the silicon wafer. **BPA** and **CB[7]** are prepared in assembly solution at a ratio of 1:4, the morphologies of which are irregular protrusion after drying on the silicon wafer. While in the 1:1 assembly solution formed by **BPA** and **CB[8]**, rhombic particles tend to be formed. Through the measurement of dynamic light scattering (Fig. 1a), the average particle size distribution of the assembly formed by **BPA** and **CB[8]** is about 1380 nm, which is consistent with the data obtained by SEM photos. The zeta potential of the assembly solution is measured as positive (Fig. 1b), indicating that the surface of particles formed by **BPA** and cucurbituril has cationic properties.

In order to explore the optical properties of **BPA** and its host–guest complexes in aqueous solution, the UV-vis absorption and photoluminescence emission experiments are performed, where 2.5% dimethyl sulfoxide (DMSO) is added to improve the solubility of **BPA** in water. The UV-vis absorption spectra of **BPA** show a series of characteristic peaks of anthracene at 359 nm, 378 nm, and 398 nm and two strong absorptions at 260 nm and 308 nm. The absorption at 308 nm shows either an intensity increase or a bathochromic shift after the addition of **CB[7]/CB[8]** (Fig. 1c). When excited at 310 nm, the **BPA** solution presents two weak fluorescence peaks at 380 nm and 430 nm assigned to the characteristic emission of 4-(4-bromophenyl)-pyridium and 9,10-diphenylanthracene, respectively (Fig. 1d), probably due to the nonradiative transition of the aggregation state between **BPA** molecules caused by the strong tendency for the accumulation of the planar extended π-system of anthracene in solution.[67] When **CB[7]** or **CB[8]** is added to the **BPA** solution, these two peaks obviously enhance (Fig. S27, ESI‡); for example, the fluorescence of **BPA** at 430 nm enhances 26.5 times with the addition of 4 equivalents of **CB[7]**,
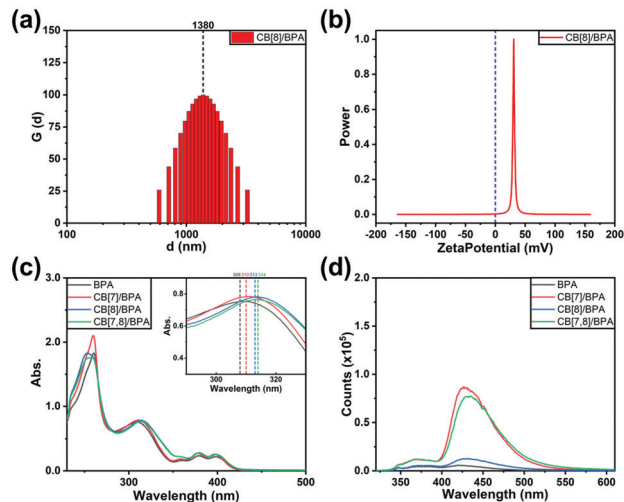

Fig. 1 (a) Dynamic light scattering of **CB[8]/BPA**, and the peak particle size of the normal distribution is about 1380 nm. (b) Zeta potential of the **CB[8]/BPA** assembly, the peak of which is at +30.8 mV. (c) UV-vis absorption spectra (illustration: partial enlarged view). (d) Prompt photoluminescence spectra (Ex. slit = 2.5 nm, Em. slit = 2.5 nm) ([**BPA**] = 0.025 mM, [**CB[7]**] = 0.050 mM and [**CB[8]**] = 0.025 mM) in water (containing 2.5% of DMSO) at 298 K (λ_{ex} = 310 nm).

probably because the binding of **CB[7]** with the 4-(4-bromophenyl)pyridinium moiety effectively disassembles the aggregated state of **BPA**. In addition, the inclusion of multiple **CB[7]** macrocycles on **BPA** molecules also increases the steric hindrance of the molecules to some extent, reduces the vibration and rotation in the fluorophore, and inhibits the nonradiative transition. These two factors jointly lead to enhanced photoluminescence. On the other hand, the larger cavity of **CB[8]** can bind two bromophenylpyridinium units at the same time, which can only partially reduce the accumulation of **BPA** molecules and slightly inhibit the non-radiative transition in molecules, leading to little enhancement in the fluorescence of guest **BPA**. Two equivalents of **CB[7]** and then one equivalent of **CB[8]** were added to **BPA** solution to explore the synergistic effects of two different sizes of cucurbituril macrocycles (**CB[7,8]/BPA**) on the photophysical behavior of **BPA**. We suspect that the addition of **CB[8]** can squeeze 2 equivalents of **CB[7]** into the alkyl chain of **BPA**, so as to further weaken the intermolecular stacking of **BPA** and weaken the non-radiative relaxation of its excited state. It is noteworthy that there exists intramolecular FRET from the phosphorescent 4-(4-bromophenyl)-pyridinium group to the fluorophore 9,10-diphenylanthracene, in which the former jumps to the single excited state (S$_1$) under the excitation of ultraviolet light, and the excitation energy of the fluorophore 9,10-diphenylanthracene matches that of the S$_1$ state of 4-(4-bromophenyl)pyridinium, and the space distance between them is also conducive to the occurrence of energy transfer. Therefore, the system crossing of bromophenylpyridinium phosphorescent groups in the S$_1$ state is blocked, and no phosphorescence is generated through the triplet excited state (T$_1$). The functional group cannot make effective ISC and enter into T$_1$. The result is that the obvious S$_1$ luminescence of 9,10-diphenylanthracene and the

This journal is © The Royal Society of Chemistry 2022

J. Mater. Chem. C, 2022, **10**, 2623–2630 | **2625**

relatively weak excited singlet luminescence of bromophenylpyridinium can be observed in the photoluminescence spectrum, and the characteristic phosphorescence emission of 4-(4-bromophenyl)-pyridium at 500 nm cannot be detected using a time-gated fluorescence spectrometer.

In order to investigate the photoreaction process of cucurbituril/**BPA** assemblies, the 365 nm UV LED flashlight is used to irradiate the experimental solution. The UV-vis absorption spectra of the solution are monitored at fixed time intervals, and a series of absorption spectra with various photoreaction times are obtained (Fig. S28, ESI‡). In these spectra, we can qualitatively and quantitatively analyze the photo-induced internal peroxycyclization of **BPA** (Fig. S29, ESI‡). The absorption intensities of three characteristic peaks of anthracene in **BPA** at 358, 376 and 395 nm gradually weaken with the extension of illumination time and are completely quenched within 50 minutes, probably because of the conversion of **BPA** to the internal peroxycyclization product **BPA$_{EPO}$**. The kinetic study demonstrates that the peroxycyclization of **BPA** follows a first-order kinetic equation process, and the reaction rate constant is 0.07728 min^{-1}. Significantly, the addition of cucurbituril can greatly accelerate the photoreaction process of **BPA**. The reaction rate constants of **CB[7]/BPA**, **CB[8]/BPA** and **CB[7,8]/BPA** are measured as 0.13751 min^{-1}, 0.22591 min^{-1} and 0.42746 min^{-1}, which are 1.8–5.5 times higher than that of free **BPA**, respectively. One possible reason is that the existence of the host cucurbituril can split the accumulation of **BPA** in water from the π–π interaction and improve the solubility to a certain extent, so as to reduce the energy dissipation of the thermal form when **BPA** is excited. This can also be explained by the enhancement of the luminescence of the solution due to the addition of cucurbituril. The molecules are stimulated to jump to S$_1$, some of which release energy in the form of fluorescence and fall back to the ground state, and the other molecules cross to T$_1$ and collide with the oxygen molecules dissolved in water to produce singlet oxygen, followed by peroxidation process of anthracene. In addition, reduced stacking can also increase the collision probability between **BPA** and oxygen species, so as to accelerate the generation and combination of singlet oxygen, which is manifested by the increase of the apparent rate constant and the decrease of the **BPA** half-life. From the change in the photoluminescence spectrum with illumination time shown in Fig. 2a, we can also find that the characteristic emission of anthracene at 430 nm gradually weakens, and the characteristic fluorescence and phosphorescence of bromophenylpyridinium gradually appear (Fig. S30, ESI‡), which also proves the existence of FRET from one point of view.

For exploring the molecular properties of **BPA$_{EPO}$** after internal peroxide cyclization in more detail and reliably, we tried to directly synthesize **BPA$_{EPO}$** and compare the properties with the **BPA** sample after the photoreaction. By adding a catalytic amount of the tetraphenylporphyrin photosensitizer to the DMSO solution of **BPA** for promoting the generation of singlet oxygen, under the irradiation of a 365 nm ultraviolet flashlight, a single-step yield of **BPA$_{EPO}$** of more than 30% can
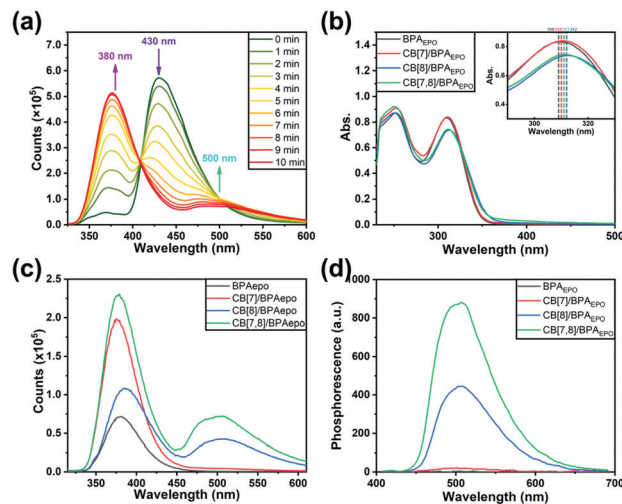

Fig. 2 The spectra of **BPA** and its host–guest complexes after photo-induced internal peroxycyclization. (a) Changes in the photoluminescence spectra of **CB[7,8]/BPA** with 365 nm UV LED flashlight irradiation time. (b) UV–vis absorption spectra (illustration: partial enlarged view). (c) Prompt photoluminescence spectra (Ex. slit = 2.5 nm, Em. slit = 2.5 nm). (d) Phosphorescence spectra (delayed by 0.2 ms, Ex. slit = 20 nm, Em. slit = 10 nm) of **BPA** (black), **CB[7]/BPA** (red), **CB[8]/BPA** (blue), and **CB[7,8]/BPA** (green) ([**BPA**] = 0.025 mM, [**CB[7]**] = 0.050 mM and [**CB[8]**] = 0.025 mM) in water (containing 2.5% of DMSO) at 298 K (λ_{ex} = 310 nm).

be achieved. By the comparison of NMR, MS, and FT-IR (Fig. S7–S9 and S31, ESI‡), it can be confirmed that the product of the photoreaction of **BPA** is the same as the synthesized **BPA$_{EPO}$**. The high-resolution mass spectrometry (HR-MS) signal of the oxidation species (Fig. S32a, ESI‡) confirmed the formation of endoperoxide. The UV-vis absorption and photoluminescence spectra of **CB[7,8]/BPA** after irradiation were very similar to those of **CB[7,8]/BPA$_{EPO}$** (Fig. S32b and c, ESI‡). In addition, the decrease of the photoreaction rate under deoxygenated conditions also confirmed that the dissolved oxygen participated in the photoreaction (Fig. S32d, ESI‡). Job's curves are measured by fluorescence spectra and UV-vis absorption spectra, confirming that the optimal bonding ratios of **BPA$_{EPO}$** to **CB[7]** and **CB[8]** are 1:4 and 1:1, respectively (Fig. S33, ESI‡). These data are consistent with the values measured from **BPA**, indicating that the photoinduced internal peroxide cyclization has no destructive effect on the molecular skeleton of **BPA$_{EPO}$**. Therefore, in the subsequent photophysical property tests, we mostly use the method of preparing solutions for the substances before and after oxidation for comparative experiments. To our surprise, different assemblies also produce different photoluminescence properties after the photo-induced internal peroxidation. After UV irradiation, the fluorescence emissions of **BPA**, **CB[7]/BPA**, **CB[8]/BPA**, and **CB[7,8]/BPA** at 430 nm disappear (Fig. 2b), while the fluorescence emissions at 380 nm greatly enhance (15.9–20.7 times), in which **CB[7,8]/BPA$_{EPO}$** gives the strongest fluorescence at 380 nm (Fig. 2c). **CB[8]/BPA$_{EPO}$** and **CB[7,8]/BPA$_{EPO}$** emit the obvious phosphorescence at 500 nm. However, under the same conditions, the phosphorescence of **CB[7]/BPA$_{EPO}$** is fairly weak, and the

2626 | J. Mater. Chem. C, 2022, **10**, 2623–2630

This journal is © The Royal Society of Chemistry 2022

phosphorescence of **BPA$_{EPO}$** is negligible (Fig. 2d, delayed 0.2 ms). After nitrogen is introduced into the solution, the phosphorescence lifetime of **CB[8]/BPA$_{EPO}$** at 500 nm increases from 133.69 μs to 289.21 μs, while that of **CB[7,8]/BPA$_{EPO}$** increases from 405.49 μs to 716.10 μs (Fig. 3a and b), confirming that the photoluminescence at 500 nm is the phosphorescence. The total quantum yields of photoluminescence (Fig. S34, ESI‡) of **CB[8]/BPA$_{EPO}$** and **CB[7,8]/BPA$_{EPO}$** are 0.78% and 1.29%, respectively. The phosphor group 4-(4-bromophenyl)pyridinium, which originally has no phosphorescence emission in aqueous solution, can form a biaxial pseudorotaxane like structure with **CB[8]**, accompanied by the green phosphorescence emission peak at 500 nm. This phenomenon is promoted by several factors: (1) the encapsulation of the **CB[8]** cavity provides a hydrophobic environment, which can protect the triplet phosphor from quenching by collision with triplet oxygen or other impurities; (2) the rigid cavity wraps two units of phosphorescent groups through a host–guest interaction, which limits their molecular motion and inhibits nonradiative relaxation; (3) the phosphorescent clusters of two molecules accumulate in the **CB[8]** cavity, resulting in a more stable π–π interaction, which promotes the occurrence of ISC; and (4) a halogen bond is formed between the C–Br of bromophenylpyridinium and the N atom of adjacent **BPA**. These factors jointly lead to the strong phosphorescence emission and the long phosphorescence life of **CB[8]/BPA$_{EPO}$** and **CB[7,8]/BPA$_{EPO}$**, while the **CB[7]/BPA** system lacks a π–π interaction and a halogen bond to promote ISC between phosphorescent groups. However, in the **BPA** molecule before the photoreaction, the characteristic absorption of the anthracene moiety just coincides with the fluorescence emission wavelength of the

phosphor group, making FRET from the singlet excited state of bromophenylpyridinium to anthracene easy to occur in **BPA**, which blocks the way of ISC. Therefore, the characteristic fluorescence of bromophenylpyridinium at 380 nm is greatly weakened, and there is no phosphorescence emission. The phosphorescence of the host–guest complex does not reappear until the internal peroxidation process induced by ultraviolet light destroys the structure of anthracene, so as to realize the purely organic RTP emission induced by the photoreaction. Then, we used phosphorescence spectrum monitoring (Fig. 3c) to explore the ability of **BPA$_{EPO}$** to decompose into **BPA** and singlet oxygen under heating conditions. After heating for 20 minutes, it can be observed that the phosphorescence intensity of **CB[7,8]/BPA$_{EPO}$** assembly solution decreases by nearly 80%, which can be partially recovered by re-illumination with a 365 nm UV LED flashlight. From the phosphorescence intensity at 500 nm, the oxidation and reduction of the assembly showed good reversible stability (Fig. 3d) under the dual stimulation of UV irradiation and prolonged heating under deoxygenated conditions.

In order to explore the potential application of the photo-reaction induced phosphorescence system in the material field, we prepared a translucent colorless hydrogel by adding a 3% mass fraction of agarose to the assembly solution after heating dissolution and then cooling. Similar to the solution state, the **BPA** molecule can undergo a photoreaction under 365 nm UV irradiation to form **BPAEPO**, which can be excited by a 302 nm light source to produce green phosphorescence. (Fig. 4a). The green phosphorescence cannot be produced without **CB[8]**, which is consistent with the results measured in solution. The mechanical properties of the hydrogel are characterized by the rheology measurement. As shown in Fig. 4b, the linear elastic–viscous area is obtained by the experiments of an
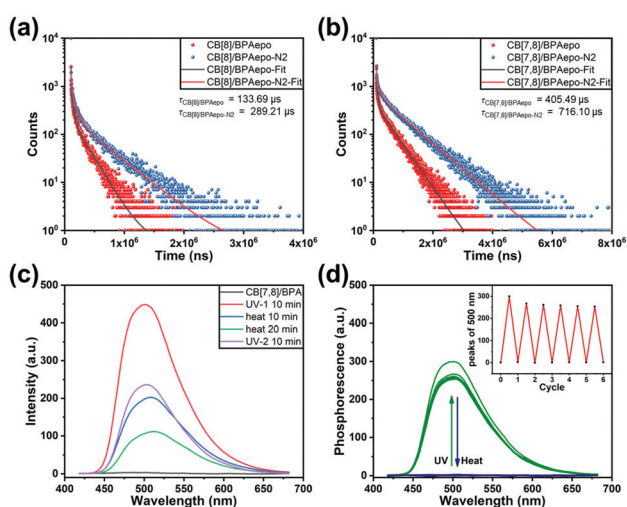
Fig. 3 Phosphorescence lifetime contrast curves for **CB[8]/BPA$_{EPO}$** and **CB[7,8]/BPA$_{EPO}$**. The phosphorescence decay curves of (a) **CB[8]/BPA$_{EPO}$**, **CB[8]/BPA$_{EPO}$**-N$_2$ and (b) **CB[7,8]/BPA$_{EPO}$**, **CB[7,8]/BPA$_{EPO}$**-N$_2$ at 500 nm at 298 K ([**BPA**] = 0.025 mM, [**CB[7]**] = 0.050 mM and [**CB[8]**] = 0.025 mM) in water (containing 2.5% of DMSO) (λ_{ex} = 310 nm). (c) Phosphorescence intensity change of **CB[7,8]/BPA** solution after irradiation, heating and re-irradiation. (d) Phosphorescence reversibility for **CB[7,8]/BPA** detected by the emission intensity change at 500 nm.
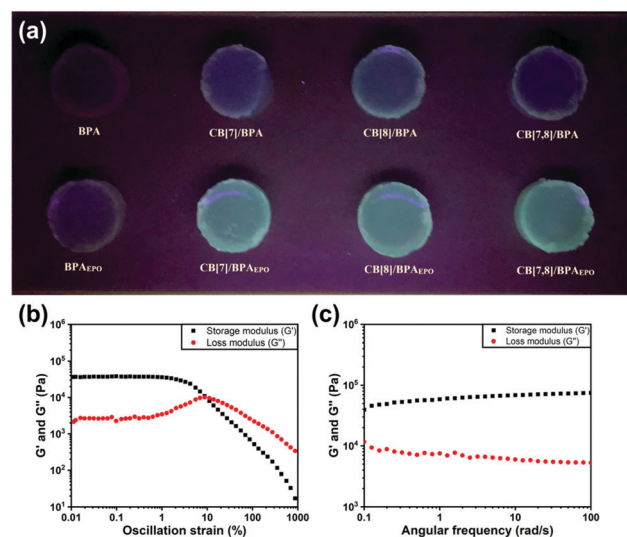
Fig. 4 (a) Agarose gel (wt% = 3%) prepared from different assembly solutions under the excitation of 302 nm in a dark environment. (b) G' (storage modulus) and G'' (loss modulus) as a function of strain. (c) G' and G'' as a function of frequency.

This journal is © The Royal Society of Chemistry 2022

J. Mater. Chem. C, 2022, **10**, 2623–2630 | **2627**

amplitude sweep at a strain (g) = 0.01–1000%. Under the strain from 0.01 to 2%, G' (storage modulus) and G'' (loss modulus) are almost constants. When the strain is greater than 2%, G' decreases, but G'' initially increases and then decreases, indicating that the hydrogel network is destroyed. With an angular frequency ranging from 0.1 to 100 rad per s, neither G' nor G'' exhibits obvious changes, and G' is always larger than G'', demonstrating good stability of the hydrogels toward the oscillation condition (Fig. 4c). These results provide the possibility for the application of BPA cucurbituril supramolecular assembly in stimulus responsive phosphorescent switching materials.

Conclusions

In summary, a photo-sensitive molecule **BPA** with 9,10-bis(4-aminophenyl)-anthracene and two bromophenylpyridinium arms was synthesized, and its host–guest complexes CB[7]/**BPA**, CB[8]/**BPA** and CB[7,8]/**BPA** were constructed. When **BPA** has not been oxidized yet, intermolecular FRET from 4-(4-bromophenyl)pyridium to 9,10-diphenylanthracene occurs, resulting in the strong fluorescence emission of supramolecular assembly at 430 nm. The addition of the rigid macrocyclic molecule cucurbituril can effectively reduce the formation of the aggregation state between **BPA** molecules, inhibit the non-radiative transition and enhance the fluorescence. Irradiation of the assembly solution with a 365 nm UV LED flashlight can induce the anthracene group in **BPA** to capture singlet oxygen and form a stable internal peroxide, thus prohibiting the FRET pathway. Such an endoperoxide can be reversibly reduced back to **BPA** by heating, so as to realize the reversible regulation of the supramolecular assembly photoluminescence. Thanks to the 1:2 inclusion of 4-(4-bromophenyl)pyridium by the host molecule, the supramolecular system with CB[8] can emit reversible green phosphorescence at 500 nm. Moreover, the addition of cucurbituril can effectively accelerate the process of the **BPA** photoreaction by about 1.8 to 5.5 times, giving this supramolecular RTP switch the rapid response capability. Finally, the successful preparation of the agarose based phosphorescent hydrogel also confirmed the application prospect of this RTP supramolecular switch construction strategy based on the anthracene photoreaction for stimulating response materials.

Experimental

Unless otherwise specified, all reagents and solvents were purchased from commercial sources and used without further purification. NMR spectra were recorded using a Bruker AVANCE III HD 400 spectrometer. Chemical shifts (δ) for ^{1}H NMR and ^{13}C NMR spectra are reported in parts per million (ppm) and relative to the solvent residual peak. Low-resolution mass (LR-MS) spectra were performed using a Bruker Autoflex III TOF/TOF200 spectrometer. High-resolution mass (HR-MS) spectra were acquired using a Varian 7.0T FTMS. The UV-vis

absorption spectrum was recorded using a Shimadzu UV-3600 spectrometer. The photo-induced endoperoxidation experiments were carried out using a photochemical reaction apparatus with a 365 nm UV LED flashlight (irradiance: 3000 mW cm^{-2}). Fluorescence and phosphorescence spectra were recorded using a Varian Cary Eclipse spectrofluorometer equipped with a plotter unit and a quartz cell (1 cm × 1 cm) at 25 °C. Quantum yields and phosphorescence lifetimes were recorded in a conventional quartz cell (10 × 10 × 45 mm) at 25 °C using an Edinburgh Instruments FS5 employing the single photon counting technique.

Solution preparation

The BPA and BPAEPO stock solution was made by dissolving them in DMSO, at a concentration of 1 mM. All the water used in this paper is deionized secondary distilled water. CB[7] and CB[8] stock solutions were dissolved in deionized water at concentrations of 1 mM and 0.25 mM, respectively. All the above stock solution was kept at 25 °C before being used. All samples used for UV-vis absorption and photoluminescence spectroscopy contain DMSO of 2.5% of the solvent volume.

Calculation of the apparent rate constant and half-life

By monitoring the UV-vis absorption spectrum of the assembly solution at 375.5 nm, a series of points with decreasing values with an increase of the illumination time were obtained. The data processing software was used to fit the exponential function of this series of points, and the formula is as follows.

$$y = a + b\mathrm{e}^{-kx},$$

where k is the apparent rate constant, and its unit is min^{-1}. Using these apparent rate constants k, the half-life $t_{1/2}$ of the supramolecular assembly can be obtained by a simple calculation.

$$t_{1/2} = \ln 2/k$$

Preparation of supramolecular RTP hydrogels

3 mL of the assembly solution was added at a concentration of 0.025 mm to the cylindrical mold. 90 mg of agarose (3% by mass of the solution) was added to the solution and stirred evenly. The mold was placed in a microwave oven for one minute heating to complete the dissolution of agarose, followed by ice water cooling for 20 minutes, and then the hydrogels can be obtained simply.

Conflicts of interest

There are no conflicts to declare.

Acknowledgements

2628 | *J. Mater. Chem. C*, 2022, **10**, 2623–2630

This journal is © The Royal Society of Chemistry 2022

Notes and references

1 Kenry, C. Chen and B. Liu, *Nat. Commun.*, 2019, **10**, 2111.
2 Y. Tao, R. Chen, H. Li, J. Yuan, Y. Wan, H. Jiang, C. Chen, Y. Si, C. Zheng, B. Yang, G. Xing and W. Huang, *Adv. Mater.*, 2018, **30**, 1803856.
3 W. Zhao, Z. He and B. Z. Tang, *Nat. Rev. Mater.*, 2020, **5**, 869–885.
4 Y. Yu, M. S. Kwon, J. Jung, Y. Zeng, M. Kim, K. Chung, J. Gierschner, J. H. Youk, S. M. Borisov and J. Kim, *Angew. Chem., Int. Ed.*, 2017, **56**, 16207–16211.
5 W. Ratzke, L. Schmitt, H. Matsuoka, C. Bannwarth, M. Retegan, S. Bange, P. Klemm, F. Neese, S. Grimme, O. Schiemann, J. M. Lupton and S. Höger, *J. Phys. Chem. Lett.*, 2016, **7**, 4802–4808.
6 R. Kabe, N. Notsuka, K. Yoshida and C. Adachi, *Adv. Mater.*, 2016, **28**, 655–660.
7 J.-H. Tan, W.-C. Chen, S.-F. Ni, Z. Qiu, Y. Zhan, Z. Yang, J. Xiong, C. Cao, Y. Huo and C.-S. Lee, *J. Mater. Chem. C*, 2020, **8**, 8061–8068.
8 S. M. A. Fateminia, Z. Mao, S. Xu, Z. Yang, Z. Chi and B. Liu, *Angew. Chem., Int. Ed.*, 2017, **56**, 12160–12164.
9 L. M. Hirvonen, M. Fisher-Levine, K. Suhling and A. Nomerotski, *Rev. Sci. Instrum.*, 2017, **88**, 013104.
10 J. Yang, X. Zhen, B. Wang, X. Gao, Z. Ren, J. Wang, Y. Xie, J. Li, Q. Peng, K. Pu and Z. Li, *Nat. Commun.*, 2018, **9**, 840.
11 X. Zhen, C. Xie and K. Pu, *Angew. Chem., Int. Ed.*, 2018, **57**, 3938–3942.
12 Q. Miao, C. Xie, X. Zhen, Y. Lyu, H. Duan, X. Liu, J. V. Jokerst and K. Pu, *Nat. Biotechnol.*, 2017, **35**, 1102–1110.
13 Y. Su, Y. Zhang, Z. Wang, W. Gao, P. Jia, D. Zhang, C. Yang, Y. Li and Y. Zhao, *Angew. Chem., Int. Ed.*, 2020, **59**, 9967–9971.
14 Z. He, H. Gao, S. Zhang, S. Zheng, Y. Wang, Z. Zhao, D. Ding, B. Yang, Y. Zhang and W. Z. Yuan, *Adv. Mater.*, 2019, **31**, 1807222.
15 Y. Su, S. Z. F. Phua, Y. Li, X. Zhou, D. Jana, G. Liu, W. Q. Lim, W. K. Ong, C. Yang and Y. Zhao, *Sci. Adv.*, 2018, **4**, eaas9732.
16 G. Chen, S. Guo, H. Feng and Z. Qian, *J. Mater. Chem. C*, 2019, **7**, 14535–14542.
17 S. Wang, H. Shu, X. Han, X. Wu, H. Tong and L. Wang, *J. Mater. Chem. C*, 2021, **9**, 9907–9913.
18 D.-A. Xu, Q.-Y. Zhou, X. Dai, X.-K. Ma, Y.-M. Zhang, X. Xu and Y. Liu, *Chin. Chem. Lett.*, 2021, DOI: 10.1016/j.cclet.2021.08.001.
19 R. Gao and D. Yan, *Chem. Commun.*, 2017, **53**, 5408–5411.
20 R. Keruckiene, D. Volyniuk, K. Leitonas and J. V. Grazulevicius, *Sens. Actuators, B*, 2020, **321**, 128533.
21 X. Yu, W. Liang, Q. Huang, W. Wu, J. J. Chruma and C. Yang, *Chem. Commun.*, 2019, **55**, 3156–3159.
22 W. Zhao, Z. He, J. W. Y. Lam, Q. Peng, H. Ma, Z. Shuai, G. Bai, J. Hao and B. Z. Tang, *Chem*, 2016, **1**, 592–602.
23 Z. Yang, Z. Mao, X. Zhang, D. Ou, Y. Mu, Y. Zhang, C. Zhao, S. Liu, Z. Chi, J. Xu, Y.-C. Wu, P.-Y. Lu, A. Lien and M. R. Bryce, *Angew. Chem., Int. Ed.*, 2016, **55**, 2181–2185.
24 L. Yang, X. Wang, G. Zhang, X. Chen, G. Zhang and J. Jiang, *Nanoscale*, 2016, **8**, 17422–17426.
25 X.-F. Wang, H. Xiao, P.-Z. Chen, Q.-Z. Yang, B. Chen, C.-H. Tung, Y.-Z. Chen and L.-Z. Wu, *J. Am. Chem. Soc.*, 2019, **141**, 5045–5050.
26 Z. Yang, C. Xu, W. Li, Z. Mao, X. Ge, Q. Huang, H. Deng, J. Zhao, F. L. Gu, Y. Zhang and Z. Chi, *Angew. Chem., Int. Ed.*, 2020, **59**, 17451–17455.
27 J. Wang, X. Gu, H. Ma, Q. Peng, X. Huang, X. Zheng, S. H. P. Sung, G. Shan, J. W. Y. Lam, Z. Shuai and B. Z. Tang, *Nat. Commun.*, 2018, **9**, 2963.
28 L. Zhan, Z. Chen, S. Gong, Y. Xiang, F. Ni, X. Zeng, G. Xie and C. Yang, *Angew. Chem., Int. Ed.*, 2019, **58**, 17651–17655.
29 E. Hamzehpoor and D. F. Perepichka, *Angew. Chem., Int. Ed.*, 2020, **59**, 9977–9981.
30 W. Ye, H. Ma, H. Shi, H. Wang, A. Lv, L. Bian, M. Zhang, C. Ma, K. Ling, M. Gu, Y. Mao, X. Yao, C. Gao, K. Shen, W. Jia, J. Zhi, S. Cai, Z. Song, J. Li, Y. Zhang, S. Lu, K. Liu, C. Dong, Q. Wang, Y. Zhou, W. Yao, Y. Zhang, H. Zhang, Z. Zhang, X. Hang, Z. An, X. Liu and W. Huang, *Nat. Mater.*, 2021, **20**, 1539–1544.
31 F. Gu, B. Ding, X. Ma and H. Tian, *Ind. Eng. Chem. Res.*, 2020, **59**, 1578–1583.
32 Z.-Y. Zhang, W.-W. Xu, W.-S. Xu, J. Niu, X.-H. Sun and Y. Liu, *Angew. Chem., Int. Ed.*, 2020, **59**, 18748–18754.
33 N. Gan, H. Shi, Z. An and W. Huang, *Adv. Funct. Mater.*, 2018, **28**, 1802657.
34 S. Kuila, K. V. Rao, S. Garain, P. K. Samanta, S. Das, S. K. Pati, M. Eswaramoorthy and S. J. George, *Angew. Chem., Int. Ed.*, 2018, **57**, 17115–17119.
35 W.-J. Fang, J.-J. Zhang, H. Zhao, J. Ni, S.-Q. Liu, Z. Liu, A.-Y. Ni, P.-P. Zhang and H.-H. Wei, *Adv. Opt. Mater.*, 2020, **8**, 2000482.
36 L. Ma, S. Sun, B. Ding, X. Ma and H. Tian, *Adv. Funct. Mater.*, 2021, **31**, 2010659.
37 Y. Zhang, L. Gao, X. Zheng, Z. Wang, C. Yang, H. Tang, L. Qu, Y. Li and Y. Zhao, *Nat. Commun.*, 2021, **12**, 2297.
38 J. Sun, J. Jia, B. Zhao, J. Yang, M. Singh, Z. An, H. Wang, B. Xu and W. Huang, *Chin. Chem. Lett.*, 2021, **32**, 1367–1371.
39 X.-Q. Liu, K. Zhang, J.-F. Gao, Y.-Z. Chen, C.-H. Tung and L.-Z. Wu, *Angew. Chem., Int. Ed.*, 2020, **59**, 23456–23460.
40 H. Liu, N. Ando, S. Yamaguchi, P. Naumov and H. Zhang, *Chin. Chem. Lett.*, 2021, **32**, 1669–1674.
41 D. Li, F. Lu, J. Wang, W. Hu, X.-M. Cao, X. Ma and H. Tian, *J. Am. Chem. Soc.*, 2018, **140**, 1916–1923.
42 X.-K. Ma, W. Zhang, Z. Liu, H. Zhang, B. Zhang and Y. Liu, *Adv. Mater.*, 2021, **33**, 2007476.
43 P. Wei, X. Zhang, J. Liu, G.-G. Shan, H. Zhang, J. Qi, W. Zhao, H. H.-Y. Sung, I. D. Williams, J. W. Y. Lam and B. Z. Tang, *Angew. Chem., Int. Ed.*, 2020, **59**, 9293–9298.
44 X.-K. Ma and Y. Liu, *Acc. Chem. Res.*, 2021, **54**, 3403–3414.
45 Y. Zhou, K. Jie, R. Zhao and F. Huang, *Adv. Mater.*, 2020, **32**, 1904824.
46 Y. Chen, F. Huang, Z.-T. Li and Y. Liu, *Sci. China: Chem.*, 2018, **61**, 979–992.
47 X.-Y. Lou and Y.-W. Yang, *Adv. Opt. Mater.*, 2018, **6**, 1800668.
48 Z.-Y. Zhang, D.-Q. Ye, Q.-Q. Gao, Z.-C. Shi, M. Xie, S.-Z. Zhan, Y.-L. Huang, G.-H. Ning and D. Li, *Inorg. Chem. Front.*, 2021, **8**, 2299–2304.

This journal is © The Royal Society of Chemistry 2022

J. Mater. Chem. C, 2022, **10**, 2623–2630 | **2629**

49 L. Zuo, G. Qin, Y. Lan, Y. Wei and C. Dong, *Sens. Actuators, B*, 2019, **289**, 100–105.

50 L. Straub, D. González-Abradelo and C. A. Strassert, *Chem. Commun.*, 2017, **53**, 11806–11809.

51 T. Li and X. Ma, *Dyes Pigm.*, 2018, **148**, 306–312.

52 X.-K. Ma, Y.-M. Zhang, Q. Yu, H. Zhang, Z. Zhang and Y. Liu, *Chem. Commun.*, 2021, **57**, 1214–1217.

53 S. Garain, B. C. Garain, M. Eswaramoorthy, S. K. Pati and S. J. George, *Angew. Chem., Int. Ed.*, 2021, **60**, 19720–19724.

54 C. Li, X. Li and Q. Wang, *Chin. Chem. Lett.*, 2021, DOI: 10.1016/j.cclet.2021.08.011.

55 Z.-Y. Zhang and Y. Liu, *Chem. Sci.*, 2019, **10**, 7773–7778.

56 Y.-H. Liu, Y.-M. Zhang, H.-J. Yu and Y. Liu, *Angew. Chem., Int. Ed.*, 2021, **60**, 3870–3880.

57 W.-L. Zhou, Y. Chen, Q. Yu, H. Zhang, Z.-X. Liu, X.-Y. Dai, J.-J. Li and Y. Liu, *Nat. Commun.*, 2020, **11**, 4655.

58 J. Wang, Z. Huang, X. Ma and H. Tian, *Angew. Chem., Int. Ed.*, 2020, **59**, 9928–9933.

59 H.-J. Yu, Q. Zhou, X. Dai, F.-F. Shen, Y.-M. Zhang, X. Xu and Y. Liu, *J. Am. Chem. Soc.*, 2021, **143**, 13887–13894.

60 J. Yang, M. Fang and Z. Li, *Acc. Mater. Res.*, 2021, **2**, 644–654.

61 X. Lin, J. Wang, B. Ding, X. Ma and H. Tian, *Angew. Chem., Int. Ed.*, 2021, **60**, 3459–3463.

62 Y. Li, F. Gu, B. Ding, L. Zou and X. Ma, *Sci. China: Chem.*, 2021, **64**, 1297–1301.

63 Y. Zhou, H.-Y. Zhang, Z.-Y. Zhang and Y. Liu, *J. Am. Chem. Soc.*, 2017, **139**, 7168–7171.

64 M. A. Filatov, S. Karuthedath, P. M. Polestshuk, H. Savoie, K. J. Flanagan, C. Sy, E. Sitte, M. Telitchko, F. Laquai, R. W. Boyle and M. O. Senge, *J. Am. Chem. Soc.*, 2017, **139**, 6282–6285.

65 Z.-Y. Zhang, Y. Chen and Y. Liu, *Angew. Chem., Int. Ed.*, 2019, **58**, 6028–6032.

66 F.-F. Shen, Y. Chen, X. Dai, H.-Y. Zhang, B. Zhang, Y. Liu and Y. Liu, *Chem. Sci.*, 2021, **12**, 1851–1857.

67 D. G. Congrave, B. H. Drummond, V. Gray, A. D. Bond, A. Rao, R. H. Friend and H. Bronstein, *Polym. Chem.*, 2021, **12**, 1830–1836.

2630 | *J. Mater. Chem. C*, 2022, **10**, 2623–2630

This journal is © The Royal Society of Chemistry 2022